Diffusion-driven and size-dependent phase changes of gallium oxide nanocrystals in a glassy host

N. V. Golubev,[a] E. S. Ignat'eva,[a] V. N. Sigaev,[a] A. Lauria,[b] L. De Trizio,[c] A. Azarbod,[de] A. Paleari*[ae] and R. Lorenzi[e]

*Corresponding authors

[a]P.D. Sarkisov International Laboratory of Glass-based Functional Materials, Mendeleev University of Chemical Technology of Russia, Miusskaya Square 9, 125047 Moscow, Russia

[b]Department of Materials, ETH Zürich, Vladimir-Prelog-Weg 5, 8093 Zurich, Switzerland

[c]Istituto Italiano di Tecnologia, Via Morego 30, 16163 Genova, Italy

[d]Department of Physics, University of Ferrara, via Saragat 1, 44100 Ferrara, Italy

[e]Department of Materials Science, University of Milano-Bicocca, via Cozzi 55, 20125 Milano, Italy

E-mail: alberto.paleari@unimib.it

Abstract

Phase transformations at the nanoscale represent a challenging field of research, mainly in the case of nanocrystals (NCs) in a solid host, with size-effects and interactions with the matrix. Here we report the study of the structural evolution of γ-Ga_2O_3 NCs in alkali-germanosilicate glass – a technologically relevant system for its light emission and UV-to-visible conversion – showing an evolution drastically different from the expected transformation of γ-Ga_2O_3 into β-Ga_2O_3. Differential scanning calorimetry registers an irreversible endothermic process at ~1300 K, well above the exothermic peak of γ-Ga_2O_3 nano-crystallization (~960 K) and below the melting temperature (~1620 K). Transmission electron microscopy and X-ray diffraction data clarify that glass-embedded γ-Ga_2O_3 NCs transform into $LiGa_5O_8$ *via* diffusion-driven kinetics of Li incorporation into NCs. At the endothermic peak, β-Ga_2O_3 forms from $LiGa_5O_8$ dissociation, following a nucleation-limited kinetics promoted by size-dependent order–disorder change between $LiGa_5O_8$ polymorphs. As a result of the changes, modifications of UV-excited NC light emission are registered, with potential interest for applications.

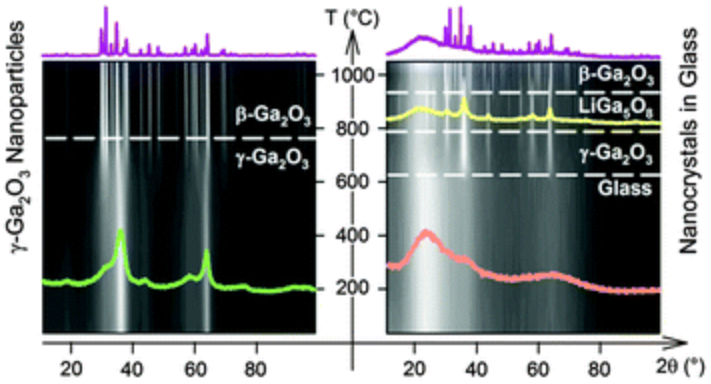

Introduction

Materials undergoing phase transformations at the nanoscale are emerging as a potential breakthrough in several technological areas. The achievement of reproducible cycles between high and low resistance phases at the submicrometer scale constitutes one of the most concrete results in the field of highly integrated rewritable data storage devices.[1] An even more challenging target is the implementation of metal–insulator transitions in wide-band-gap nanosystems, as found in Ga-oxide upon amorphous-to-crystalline phase changes.[2] Recent results regarding Ga containing oxide glasses suggest that optical properties – such as UV transmittance and UV excited light emission – can be conveniently modified by crystallization of Ga-oxide nanoparticles incorporated in the glass matrix.[3–5] These results enable the use of nanocrystal (NC) growth – and NC phase changes inside a solid host – as a tool for functionalizing glass-based materials for information technology. The idea of achieving unprecedented data-storage capability and stability by inducing local modifications of structural and optical functions in glass – specifically by means of focused laser exposure – has recently been envisaged and preliminarily demonstrated in a prototypal system of silica glass.[6] Promising results have also been obtained for silver-containing phosphate glass through the formation of fluorescent Ag clusters under laser exposure.[7] As regards nanostructured glasses, the knowledge of the phase changes that NCs undergo in a solid matrix is important for evaluating possible strategies of nanocrystal-in-glass data-storage and their real potential.

The detailed mechanisms underlying structural phase changes at the nanoscale are not easily predictable in general,[8,9] and particularly when the process involves NCs interacting with a solid host.[10–13] This is the case of Ga oxide NCs in silicate glass, which is one of the prototypal systems of oxide-in-oxide nanostructured glasses together with SnO_2-doped silica.[14] Stability and thermal evolution of Ga-oxide nanophases are expected to be largely different from the freestanding and pure compound. The role of a solid host in the incorporation of doping species inside Ga_2O_3 NCs has been recently investigated,[15] but also the structural evolution of Ga_2O_3 is expected to be influenced. In fact, in glass, Ga-oxide can segregate in a crystal phase different from the thermodynamically stable β-Ga_2O_3 structure.[3,4,16,17] Distinct Ga-oxide polymorphs are reported in the literature, indicated as α, β, γ, δ, ε, and κ, with quite different structures and stability properties.[18,19] Among these phases, β-Ga_2O_3 is the thermodynamically stable one, with monoclinic structure.[20] The α-Ga_2O_3 phase crystallizes in the structure of corundum, and single crystals can only be grown under specific conditions of temperature and pressure.[21] γ-Ga_2O_3 shows a cubic spinel-type structure, analogous to γ-Al_2O_3.[22,23] It can be prepared as powder or nanopowder, either from a high temperature calcination process of gallia gel,[22–24] or through solution-based syntheses from organic molecular precursors.[25,26] γ-Ga_2O_3 irreversibly transforms into β-Ga_2O_3*via* a two step phase change involving an intermediate reversible change into a γ′-Ga_2O_3 phase.[27] δ-Ga_2O_3 was first observed as a result of heating of evaporated gallium nitrate solution at 470–520 K.[28] It was identified as a distinct polymorph with C-type rare earth sesquioxides,[28] but new recent data suggest that δ-Ga_2O_3 is probably a nanocrystalline form of ε-Ga_2O_3 and not a distinct polymorph.[19] This metastable phase in

fact transforms into orthorhombic ε-Ga_2O_3 after heating above 770 K. Heating of ε-Ga_2O_3 above 1140 K eventually leads to stable β-Ga_2O_3.[28]

In glass, phase separation and crystallization of Ga oxide nanophases in the amorphous matrix has been investigated in recent years by different groups with the aim of studying the possible crystalline nanosystems that are able to host optically active ions with particularly efficient IR light emission.[29–34] In these studies different Ga oxide structures have been stabilized in glass. Interestingly, the reported results show that, besides β-Ga_2O_3,[29–33] γ-Ga_2O_3 can also grow in the form of embedded NCs in oxide glasses,[3–5,33] occasionally with additional mixed oxides such as $LiGa_5O_8$, $LiGaSi_2O_6$, when lithium is present in the matrix, or $(Ga_2O_3)_3(GeO_2)_2$.[35–38] The composition of the initial glass plays a clear role in determining the resulting Ga-oxide nanophase. In lithium germanosilicate glasses, we have recently found that the growth of γ-Ga_2O_3 NCs proceeds from secondary phase separation and crystallization of native Ga-rich nano-heterogeneities generated by liquid–liquid phase-separation during glass quenching.[4] This result prospects the possibility of tailoring the NC size by controlling the nucleation process. At the moment, however, no detailed information is available on the stability range and phase transformations of γ-Ga_2O_3 NCs – as well as of the other related Ga-oxide nanophases – when embedded in a glass matrix, despite their importance in possible applications.

In this article we fill the gap of knowledge on thermal stability and phase changes of γ-Ga_2O_3 after its emergence as NCs in an amorphous solid host. A specific Ga-containing alkali–germanosilicate glass has been chosen to assure phase separation of γ-Ga_2O_3 NCs with a not too large mean NC size and concentration, so as to avoid detrimental light scattering in the view of optical applications. For this purpose, the selected glass comprises an amount of Ga_2O_3 larger than 15 mol% (a value we verified to be not enough to promote NC formation at relatively low temperature) and significantly lower than 30 mol% (a concentration we observed to give rise to strong light scattering from phase separation even in as-quenched glass). The investigated glass also includes GeO_2 – in equal amount of SiO_2 – to lower melt viscosity and melting temperature with respect to the pure silicate (about 100 K lower than in GeO_2-free variant), and alkali ions to provide partial charge compensation for Ga substituting for Si and Ge in the glass.

Starting from the comparison between thermally induced changes in γ-Ga_2O_3 nanopowder and γ-Ga_2O_3 nanophase in glass, our investigation gives an insight into the role of the solid alkali-oxide host in the structural evolution of Ga-oxide guest nanophases. The investigation highlights a complex and still unrevealed evolution through reactions with alkali ions diffusing from the matrix, resulting in structural changes and decomposition. Our results show for the first time the formation of β-Ga_2O_3 from embedded γ-Ga_2O_3*via* Li diffusion and formation of the $LiGa_5O_8$ spinel phase. The data suggest a relationship between the endothermic process that gives rise to β-Ga_2O_3 and the order–disorder change of $LiGa_5O_8$, whose occurrence turns out to be influenced by size-effects and eventually promotes $LiGa_5O_8$ dissociation into β-Ga_2O_3. The analysis of the role of the Li/Na ratio and of NiO as a crystallizing agent is used to verify the model of reactions extracted from measurements at different temperatures and from isothermal analysis of the structural evolution of the nanostructured glass. As a result, the data give a tool for a clear design of stability and changes of the embedded crystal phase. Finally, taking into account some recent results on the light emission properties of γ-Ga_2O_3 NCs in glass,[3] we analyze the photoluminescence (PL) of the obtained nanophases, providing a basis for the evaluation of a phase-controlled strategy for tailoring optical functions of Ga-oxide containing glass-based systems.

Experimental procedure

Preparation of nanostructured glasses

Glasses with nominal composition $7.5Li_2O–2.5Na_2O–20Ga_2O_3–35GeO_2–35SiO_2$ (mol%) were prepared through the conventional melt-quenching method. The raw materials were amorphous

SiO_2 (special purity grade), GeO_2 (special purity grade), Li_2CO_3 (chemically pure), Na_2CO_3 (chemically pure), and Ga_2O_3 (chemically pure). For comparison purpose, glasses with composition different from the abovementioned one were also synthesized. In the case of Ni-containing samples, the NiO reagent (analytical grade) was added. The amount of reagents in each batch was calculated in order to prepare 20–70 g of the final product. The starting materials were weighed using an analytical balance with an accuracy of 0.001 g. In each preparation, the raw powders were thoroughly mixed in a beaker for 15–20 min. The glasses were prepared in an uncovered platinum crucible (~45 ml) in an electrically heated furnace at a temperature of 1753 K for 40 min. The melt was poured onto a stainless steel plate and quenched by pressing with another stainless steel plate to obtain samples of about 2 mm of thickness. The as-quenched glass was cut to the desired shape with a low-speed diamond saw or a grinding disc using water as a coolant. Samples were then polished for optical measurements or ground for powder diffraction or electron microscopy analysis.

For *ex situ* characterization of structural modifications, part of the as-quenched bulk samples was heat-treated in a muffle at various temperatures according to data obtained from differential scanning calorimetry (DSC) analysis. In such cases, heat treatments were performed, with an accuracy of the temperature control within ±2 K, either placing the samples into the furnace at room temperature or directly at the treatment temperature. The latter procedure was used for prolonged isothermal treatments as a function of the treatment duration. Instead, to identify the crystalline phases formed at the extrapolated onset and peak extremum temperatures in DSC curves, samples were treated at room temperature with the same heating rate as in DSC measurements. After treatment, the samples were quenched after removing them from the furnace either immediately, in the case of treatment at extrapolated peak onset temperature, or after staying for 10 min, in the case of treatment at the DSC peak extremum temperature.

$LiGa_5O_8$ and γ-Ga_2O_3 reference samples

$LiGa_5O_8$ was prepared by solid state reaction. Raw materials were ground together in an agate mortar and then sintered at 1273 K for 16 h in air. Nanopowder of γ-Ga_2O_3 was synthesized *via* a non-aqueous sol–gel route.[39] 1 g of gallium(III) acetylacetonate was dissolved in 20 ml of anhydrous benzyl alcohol in a glovebox (O_2 < 0.1 ppm and H_2O < 0.1 ppm). The solution was then poured in a 45 ml PTFE liner and transferred to a steel autoclave (Parr Instrument Company) and hermetically sealed. The autoclave was removed from the glove box and stored in a heated furnace at 473 K for 2 days. The resulting milky suspension was centrifuged and the obtained precipitate was carefully washed with diethyl ether, and dried in air at 333 K for 12 hours. Eventually, to completely remove any organic residual, powders were heated in air at 693 K for 1 h.

Material characterization

DSC measurements from room temperature up to about 1470 K were performed on a Netzsch DSC 449F3 high-temperature thermoanalyzer in a platinum pan with cover, at a heating rate of 10 K min^{-1} in Ar, using bulk samples of 10–15 mg. The reproducibility of endothermic and exothermic peak extremum temperature in the investigated samples is within 2 K.

X-ray diffraction patterns of powdered samples were recorded on a D2 Phaser diffractometer (Bruker) employing nickel-filtered CuKα radiation. High-temperature diffraction patterns were obtained from 300 to 1470 K using a diffractometer X'Pert PRO (PANalytical) equipped with a high-temperature X-ray diffraction chamber model HTK 1200 (Anton Paar). A heating rate of 10 K min^{-1} was used during *in situ* XRD measurement, with a stasis of 10 min before scanning, each with a duration of about 20 min. Crystalline phases were identified by comparing the peak position and relative intensities in the X-ray diffraction pattern with the ICDD PDF-2 database. A Tecnai G2 F20 transmission electron microscope, equipped with a Schottky gun operated at 200 kV acceleration

voltage, was used to acquire high angle annular dark field (HAADF)-scanning TEM (STEM) images of the samples.

Photoluminescence spectra were obtained upon excitation at 250 nm using a xenon lamp and a MS2004i SOL instruments Ltd (Belarus) monochromator with a bandwidth of 4 nm and collecting the emitted light through a second monochromator MS3504i SOL instruments Ltd with a spectral resolution of 2 nm and a photosensor module H7844 Hamamatsu.

Results and discussion

Thermal evolution of glass and the nanophase

The DSC curves in Fig. 1 give a first insight into the main features of the thermal evolution of the mixed oxide system, including the effects of nickel doping and the changes in the Li/Na ratio with respect to the composition $7.5Li_2O–2.5Na_2O–20Ga_2O_3–35GeO_2–35SiO_2$. Such variants give us a tool for checking the role of Li and Na ions in the structural changes, also comparing the induced effects with those caused by NiO addition as the crystallizing agent. In all the investigated compositions we register the occurrence of an exothermic peak in the temperature range 945–1010 K, about 110–130 K above the glass transition temperature, evidenced by a smooth step in the DSC curves. In addition, at higher temperatures (in the range 1280–1335 K), almost all the samples undergo an endothermic process, except Li-free materials. Lithium removal indeed causes a relevant modification of the thermal evolution. The exothermic peak significantly shifts to higher temperature, a second exothermic peak is observed just above 1200 K, whereas no endothermic process occurs. By contrast, sodium removal from the composition does not drastically change the first steps of the thermal evolution (glass transition and exothermic peak), but it moves the endothermic process towards higher temperatures. Interestingly, a similar shift of the endothermic peak is observed as a result of nickel addition, even though, in that case, it is accompanied by an opposite minor shift of the exothermic peak towards lower temperature.

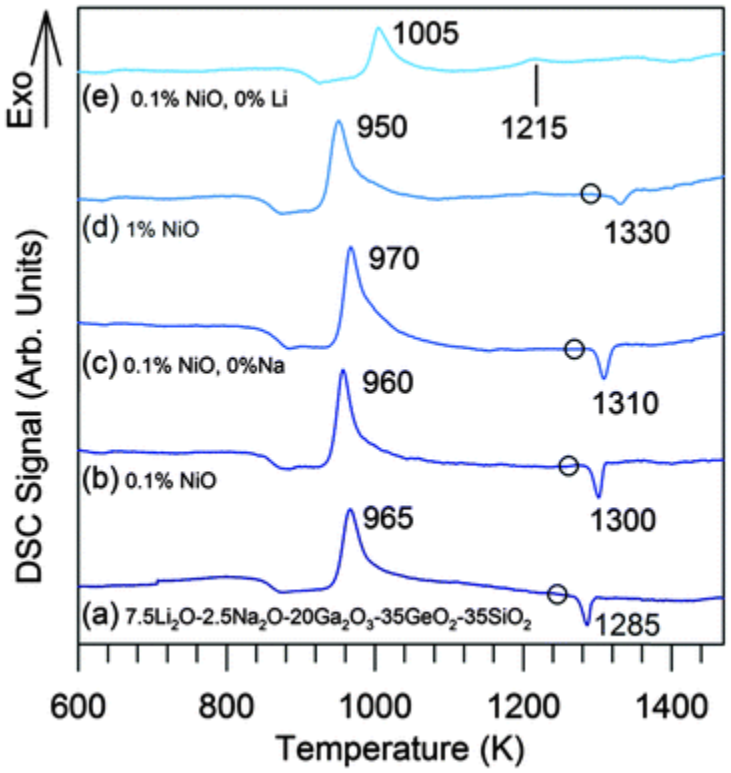

Fig. 1 DSC curves of glasses with molar composition, (a) $7.5Li_2O–2.5Na_2O–20Ga_2O_3–35GeO_2–35SiO_2$; (b) $7.5Li_2O–2.5Na_2O–20Ga_2O_3–35GeO_2–35SiO_2$ doped with 0.1NiO; (c) $10Li_2O–20Ga_2O_3–35GeO_2–35SiO_2$ doped with 0.1NiO; (d) $7.5Li_2O–2.5Na_2O–20Ga_2O_3–35GeO_2–35SiO_2$ doped with 1NiO; and (e) $10Na_2O–20Ga_2O_3–35GeO_2–35SiO_2$ doped with 0.1NiO. Circles indicate the treatment temperatures (at T_{ep} −40 K) considered in isothermal treatments. Curves are vertically shifted for clarity.

In any case, apart from such differences (discussed in more details in a next section), such a preliminary analysis shows that the observed succession of exothermic and endothermic processes is an intrinsic feature of the investigated mixed Li–Ga–Ge–Si oxide system, quite independent of doping and partial alkali substitution, whereas fully Na-substituted Li-free composition does not undergo the endothermic process, even with NiO addition. The first exothermic peak at about 970 K has recently been associated with crystallization of γ-Ga_2O_3 in the amorphous alkali–germanosilicate matrix.[4] By contrast, no study has been carried out so far on the endothermic process registered in Fig. 1. The analysis of the compositional variants gives some preliminary information. Li_2O, with respect to Na_2O, promotes phase separation in the investigated glass composition and plays a key factor in the mechanisms taking place in the endothermic process.

The XRD patterns and TEM images reported in Fig. 2 – collected at room temperature on samples heated at representative temperatures based on the DSC data – provide an overview of the structural and morphological changes occurring in the crystalline nanophase. For comparison, we report the XRD pattern of as-quenched glass (curve 1 in Fig. 2a), consisting of a broad amorphous halo only, and of material treated at the exothermic peak temperatures (curve 2 in Fig. 2a), in which we observe reflections ascribable to γ-Ga_2O_3, as previously reported.[4] The treated sample is transparent (Fig. 2b), as the initial glass, in spite of the segregation of the crystalline γ-Ga_2O_3 phase evidenced in the XRD pattern. TEM analysis indeed displays a large concentration of embedded NCs of few nm (5 ± 2 nm from TEM images in Fig. 2c).

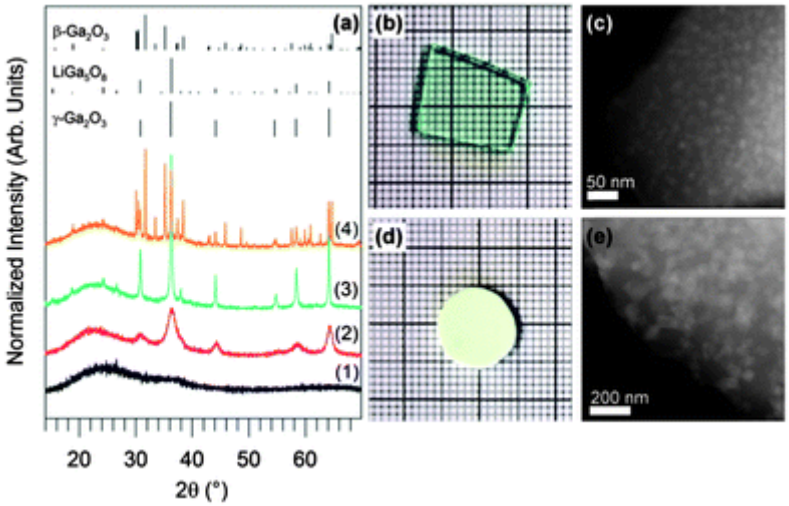

Fig. 2 (a) XRD patterns of $7.5Li_2O–2.5Na_2O–20Ga_2O_3–35SiO_2–35GeO_2$, doped with 0.1NiO, (1) as-quenched from the melt, (2) after 5 hours at 960 K, (3) 1 hour at 1210 K, and (4) heated at 10 K min^{-1} from 300 to 1300 K with a final stay of 10 min before quenching. XRD patterns are vertically shifted for clarity. Reflections of γ-Ga_2O_3, $LiGa_5O_8$, and β-Ga_2O_3 phases are indicated by sticks, according to PDF files ICDD PDF2 #00-020-0426, ICDD PDF2 #01-076-0199, and ICDD PDF2 #00-041-1103, respectively. (b) Photo and (c) HAADF-STEM images of the material after treatment at the exothermic peak temperature for 15 min. (d) Photo and (e) HAADF-STEM images after treatment at 1210 K.

After heating at a temperature close to the extrapolated endothermic peak onset temperature, we register (curve 3 in Fig. 2a) additional lines (specifically at 15.3°, 24.2°, 26.6°) consistent with the occurrence of the $LiGa_5O_8$ spinel phase. The sample is not transparent (Fig. 2d). TEM analysis shows the occurrence of bigger crystals, several tens of nanometers in size, with a well defined cubic crystal habit (TEM image in Fig. 2e).

$LiGa_5O_8$ is strictly related to γ-Ga_2O_3 through a partial substitution of Li ions for Ga ions in octahedral crystallographic sites.[38] Interestingly, XRD analysis of samples treated for 10 min at 1300 K (curve 4 in Fig. 2a) indicates that the final result of the process registered by the DSC endothermic peak is not the phase change from γ-Ga_2O_3 to $LiGa_5O_8$, but instead the formation of β-Ga_2O_3.

Embedded nanocrystals *vs.* nanopowders

The link between the endothermic process and the formation of β-Ga_2O_3, just pointed out from the data in Fig. 1 and 2, cannot be immediately ascribed to the expected evolution of the involved crystalline phase and gives a somewhat counterintuitive result. In fact, on the one hand, monoclinic β-Ga_2O_3 is by far more stable than spinel γ-Ga_2O_3, and the spinel-to-monoclinic transformation is thus expected to reduce the energy of the system with a resulting exothermic process which cannot justify the endothermic peak observed in DSC. On the other hand, at about 1410 K, $LiGa_5O_8$ is known from early studies to undergo an endothermic process of transformation to a high temperature polymorph,[40] analogously to other spinel compounds.[41] Low- and high-*T* polymorphs are strictly related to each other, the low-*T* one being an ordered superstructure of the high-*T* phase.

To verify what kind of thermal evolution the involved phases would undergo separately (not embedded in a matrix) with respect to the glass embedded nanophase, we carried out a direct comparison between the changes observed in *in situ* XRD measurements at different temperatures up to 1475 K in the reference samples of γ-Ga_2O_3 nanopowder from solution-based synthesis and $LiGa_5O_8$ powder from solid state reaction (Fig. 3a and b, respectively) and in nanostructured γ-Ga_2O_3-containing glass (Fig. 4). The transformation of γ-Ga_2O_3 nanopowder into β-Ga_2O_3 occurs at about 1100 K, whereas $LiGa_5O_8$ undergoes a polymorphic transformation at about 1430 K (Fig. 3c and d, respectively). The transformation occurring in $LiGa_5O_8$ is reversible and appears as an endothermic DSC peak by heating and an exothermic peak by cooling. The responsible structural transformation involves a change from a low temperature ordered phase to a less ordered one whose XRD pattern shows the lack of several reflections of the low temperature phase originating from ordering-related superstructures.[40] The data of nanostructured glass in Fig. 4 show that $LiGa_5O_8$ co-exists with γ-Ga_2O_3 (see data collected at 1175 K), before the formation of β-Ga_2O_3 that starts to be detected at 1275 K, accompanied by the endothermic DSC peak. Importantly, this process is not reversible and, in fact, no exothermic peak is observed by cooling (the DSC curve during cooling is not shown). Therefore, the endothermic peak in the range 1280–1335 K cannot be ascribed to a reversible polymorphism of the formed $LiGa_5O_8$. Finally, heating at 1750 K, re-melting gives rise to the initial glass with the same thermal evolution through γ-Ga_2O_3, $LiGa_5O_8$ and β-Ga_2O_3.

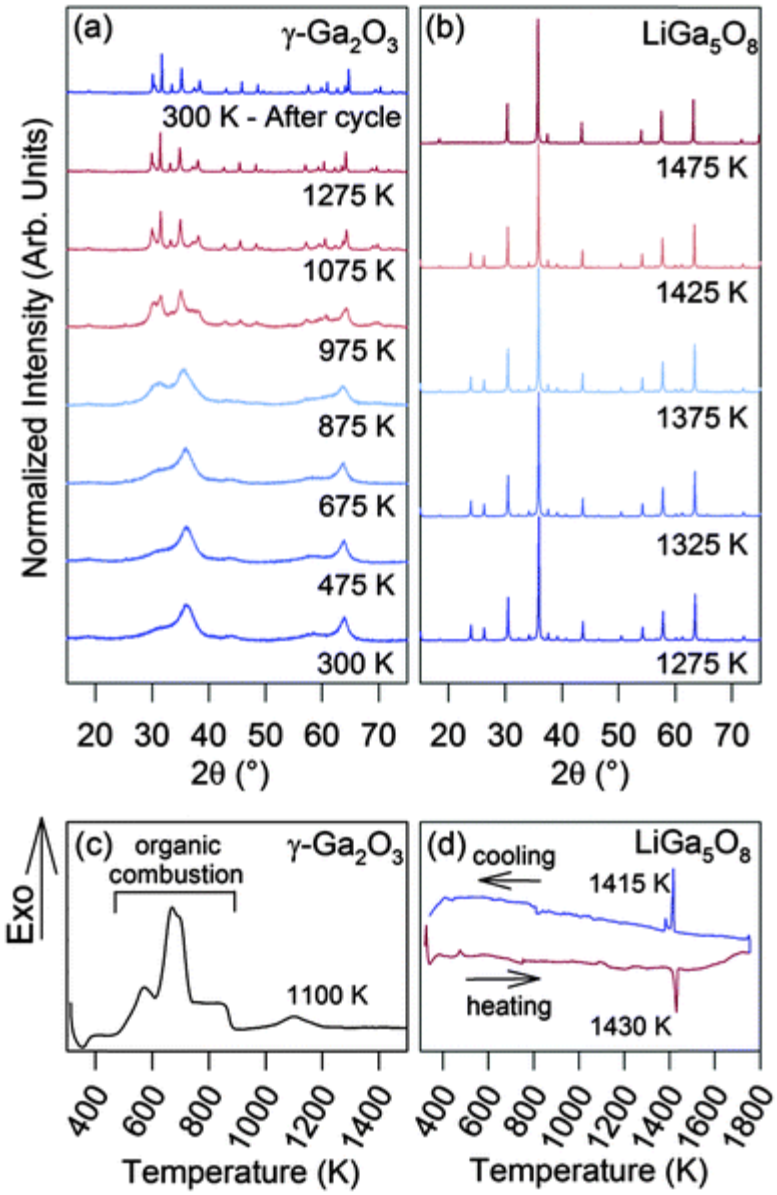

Fig. 3 XRD patterns at increasing temperature of (a) γ-Ga_2O_3 and (b) $LiGa_5O_8$ reference powder samples. Patterns are vertically shifted for clarity. DSC curves of the same samples are displayed in (c) and (d), respectively.

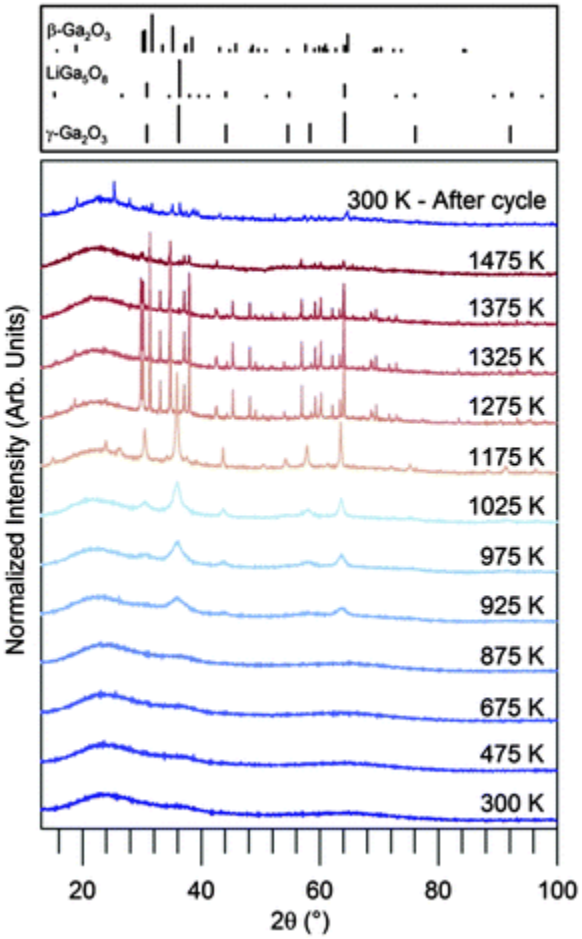

Fig. 4 *In situ* XRD of $7.5Li_2O–2.5Na_2O–20Ga_2O_3–35GeO_2–35SiO_2$ doped with 0.1 of NiO, measured at the indicated temperature. XRD patterns are vertically shifted for clarity.

The results in Fig. 3 and 4 point out the crucial role of the interactions between the nanophase and the matrix in the thermal evolution of the embedded NCs. In fact, the registered changes do not correspond to any feature encountered in the transformation paths of γ-Ga_2O_3 and $LiGa_5O_8$ phases separately. Specifically, there is no exothermic process of γ-Ga_2O_3 transformation into β-Ga_2O_3. Furthermore, the $LiGa_5O_8$ phase disappears in concomitance with β-Ga_2O_3 growth during an endothermic process not ascribable to $LiGa_5O_8$ polymorphism alone.

Isothermal heating and reaction kinetics

Data from isothermal heating experiments at about 1210 K provide us a deeper insight into the relationships among the crystalline phases identified along the thermal evolution of the glass-embedded NCs. In Fig. 5 we show XRD patterns collected at 300 K on nanostructured glasses heated at 1210 K with duration times increasing from 0.5 to 160 hours.

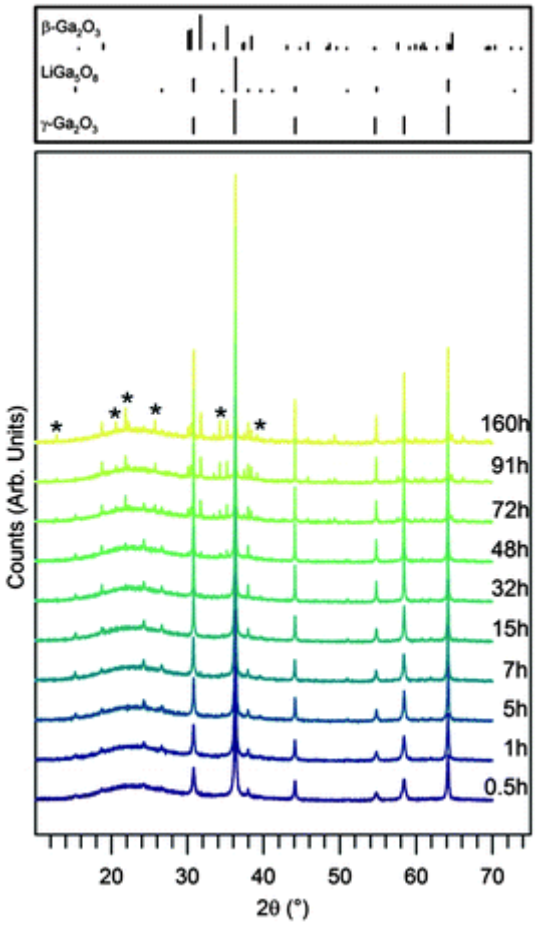

Fig. 5 XRD results on $7.5Li_2O–2.5Na_2O–20Ga_2O_3–35GeO_2–35SiO_2$ doped with 0.1 of NiO after isothermal heating at 1210 K for the indicated duration time. XRD patterns are vertically shifted for clarity. Reflections ascribable to a minor amount of $LiGaGeO_4$, according to PDF files ICDD PDF2 #01-079-0213, are indicated by asterisks.

The data, obtained after prolonged heating at a temperature lower than the endothermic peak, give us the possibility to follow the relevant processes on a time scale easy to be controlled experimentally. From Fig. 5, we see main effects on the progressive transformation of the γ-Ga_2O_3 XRD pattern into that of $LiGa_5O_8$, and the appearance of the β-Ga_2O_3 reflections which reveals early growth. Additional reflections of minor intensity, ascribable to $LiGaGeO_4$, become detectable after very long treatments (>72 h) in the final steps of the isothermal heating experiment (see stars in Fig. 5). Therefore, we can argue that Li_2O does not permanently re-dissolve in the glass after β-Ga_2O_3 formation but instead shows some very slow back reactivity with the Ga-oxide component.

However, no evidence of such reflections is registered in any other measurement, neither in *ex situ* nor in *in situ* experiments even on samples treated at temperatures higher than 1210 K. The formation of $LiGaGeO_4$ can thus be assigned to very slow processes which do not take part in the main thermal evolution of the nanophase, and it will not be discussed further. As regards the main transformation of γ-Ga_2O_3 into $LiGa_5O_8$, the experimental intensity ratio R_{exp} between the main reflections at 64.2° and 36.3° – occurring in both γ-Ga_2O_3 and $LiGa_5O_8$ patterns but with different intensity ratios (R_γ and R_{Li}, respectively) – turns out to be a quite sensitive parameter for a semi-quantitative estimation of the change of the relative amount of these phases.

In the approximation of simple additive relationship $I_{64°,36°}|_{exp} = a_\gamma I_{64°,36°}|_\gamma + b_{Li} I_{64°,36°}|_{Li}$ between the intensity $I_{64°,36°}$ of reflections at 64.2° and 36.3° (where a_γ and b_{Li} practically coincide with the relative amounts of γ-Ga_2O_3 and $LiGa_5O_8$ respectively, considering that the diffraction densities of the two phases differs by less than 4%), we obtain $b_{Li} = R_{Li}[1 - R_\gamma/R_{exp}]/[R_{Li} - R_\gamma]$, with $a_\gamma + b_{Li} = 1$. In Fig. 6, we report the amount of [$LiGa_5O_8$] normalized to the total amount of the two Ga-oxide

phases (*i.e.* b_{Li}) for different isothermal treatment durations. The formation of $LiGa_5O_8$ follows a kinetics that is consistent with a 3-dimensional diffusion-driven mechanism, as expected in a process mostly induced by Li diffusion from the glass matrix. The data of $LiGa_5O_8$ formation can in fact be reproduced by Jander's equation of 3D diffusion reaction for spherical particles,[42]

$$[1 - (1 - b_{Li}(t))^{1/3}]^2 = kt \quad (1)$$

with $k = 8 \times 10^{-7}$ s^{-1}. In the inset of Fig. 6, we also report the cubic root of the relative amount of decreasing γ-Ga_2O_3 phase, $[1 - b_{Li}(t)]$, linearly fitted as a function of $t^{1/2}$. Instead, the growth of the β-Ga_2O_3 phase – monitored by the XRD intensity at 35.2° *vs.* heating time at 1210 K as reported in Fig. 6 – follows a sigmoid along the isothermal experiment.

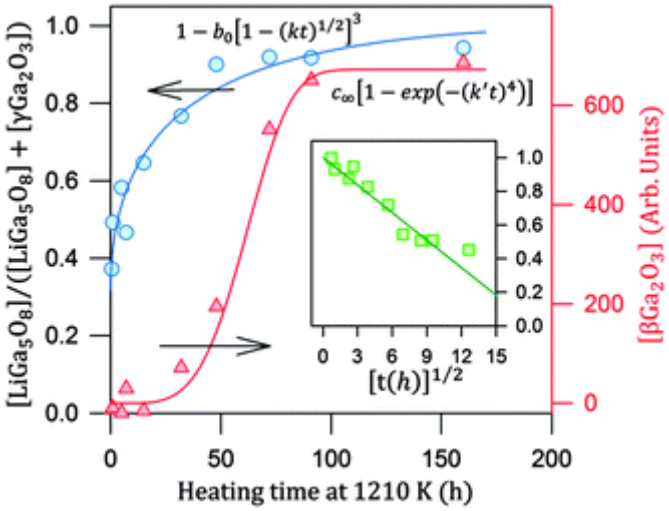

Fig. 6 Variations of the crystalline phases after isothermal treatments at 1210 K *vs.* time in $7.5Li_2O–2.5Na_2O–20Ga_2O_3–35GeO_2–35SiO_2$ from XRD data of Fig. 5. $LiGa_5O_8$ (circles), β-Ga_2O_3 (triangles), and γ-Ga_2O_3 (squares) are reported, respectively, normalized to the total amount of Ga-oxide phases, in arbitrary units, and normalized to the maximum value. Curves are the results of the fit with the indicated functions from the kinetic expression in eqn (1) and (2).

Such a behaviour is encountered in solid-state processes with nucleation mechanisms undergoing restrictions on the growth of the number of nuclei.[42] These restrictions – typical of solid-state decomposition and mainly related to coalescence between nucleation sites during the process – eventually cause a change of sign in the rate dN/dt of the nuclei number, corresponding to the inflection point of the sigmoid in the kinetics of transformation. As a matter of fact, the data can be fitted by an Avrami–Erofeyev equation for a 3-dimensional single-step nucleation process,[42]

$$[-\ln(1 - \beta(t))]^{1/4} = k't \quad (2)$$

where β is proportional to the amount of β-Ga_2O_3 phase, and $k' = 4 \times 10^{-6}$ s^{-1}. It is worth noting that the diffusion-driven γ-Ga_2O_3-to-$LiGa_5O_8$ kinetics and the kinetics of the β-Ga_2O_3 growth are not directly related to each other. In fact, the decrease of γ-Ga_2O_3 with the formation of $LiGa_5O_8$ – through Li-diffusion from the matrix – comes to completion when only a minor fraction of the total Ga oxide component in the material is transformed into β-Ga_2O_3 (see XRD data in Fig. 5). The modification of γ-Ga_2O_3 into $LiGa_5O_8$ indeed starts to occur (*in situ* XRD data in Fig. 4) well below the temperature of the endothermic peak registered in DSC measurements that is related to the formation of β-Ga_2O_3. In Fig. 7 we report the changes in the XRD amplitude and FWHM of the reflection at 36.3° (occurring both in γ-Ga_2O_3 and $LiGa_5O_8$) along the isothermal experiment. The

data suggest that the sum of the two phases does not change relevantly, so confirming that their changes are strictly correlated with each other without intervention of any transformation into β-Ga_2O_3. In other words, β-Ga_2O_3 is not directly involved in the disappearance of γ-Ga_2O_3. Rather, the isothermal heating experiment points out that the formation of β-Ga_2O_3 is the result of some kind of subsequent evolution of $LiGa_5O_8$ during the endothermic process.

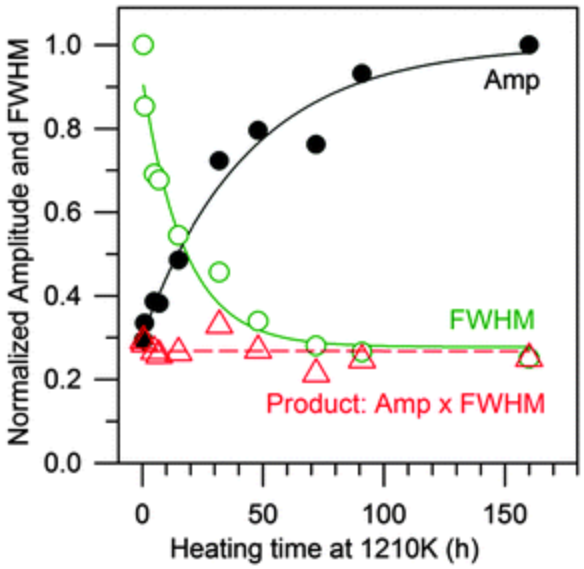

Fig. 7 Full width at half maximum (FWHM, open circles) and amplitude (Amp, filled circles) of reflection at 36.3° (common to γ-Ga_2O_3 and $LiGa_5O_8$) in XRD patterns in Fig. 5 of samples undergoing an isothermal heating experiment. The product of their values is also reported (triangles).

The endothermic process

As a result of the isothermal heating experiment, the origin of the endothermic process in the range 1280–1335 K appears strictly connected with the $LiGa_5O_8$ phase. However, as we have directly verified in the reference $LiGa_5O_8$ sample (Fig. 3), the only known transformation $LiGa_5O_8$ undergoes is a reversible change into a high temperature polymorph, occurring at about 1410 K in bulk material.[40] Remarkably, no certain information is instead available, to the best of our knowledge, about the melting temperature of $LiGa_5O_8$, which anyways should be above 1720 K.[40,43] Actually, from 1410 K up to the melting point, the high temperature polymorph is not completely stable, and indications of decomposition with loss of lithium were reported after prolonged treatment above 1420 K.[44] In that temperature region, decomposition was observed to be accompanied by detection of weak β-Ga_2O_3 XRD reflections. Incidentally, such a propensity to decompose is consistent with the indication of incongruent melting of $LiGa_5O_8$ reported in an early study on the phase diagram of the Li_2O–Ga_2O_3–B_2O_3 system.[45] Ultimately, all these observations suggest that the structural instability of $LiGa_5O_8$ at high temperature and its tendency to decompose with lithium release (according to the reaction $2LiGa_5O_8 \rightarrow 5\beta\text{-}Ga_2O_3 + Li_2O$) can play a role in the endothermic process at about 1300 K, despite its very high melting temperature. In other words, the endothermic peak – anticipated and prepared at a slightly lower temperature by diffusion-driven formation of $LiGa_5O_8$ from γ-Ga_2O_3 NCs – gives rise to β-Ga_2O_3 NCs through a process that likely involves $LiGa_5O_8$ decomposition. Such an analysis, however, poses the problem of the quite low temperature of the endothermic peak, which does not fall in, and it is definitely lower than the reported temperature range of $LiGa_5O_8$ decomposition. It is indeed lower than the order–disorder transition from the low temperature polymorph to the high temperature one. Nevertheless, the reduced NC size and the

constraints imposed by the matrix can play a role in reducing the temperature of the process responsible for the nanophase destabilization.

We can evaluate the role of the NC size in the endothermic peak comparing samples modified by the presence of crystallizing agent such as Ni or additional Li, as in the set of samples in Fig. 1, so as to give rise to $LiGa_5O_8$ NCs with different size at the onset of the endothermic process (Fig. 8).

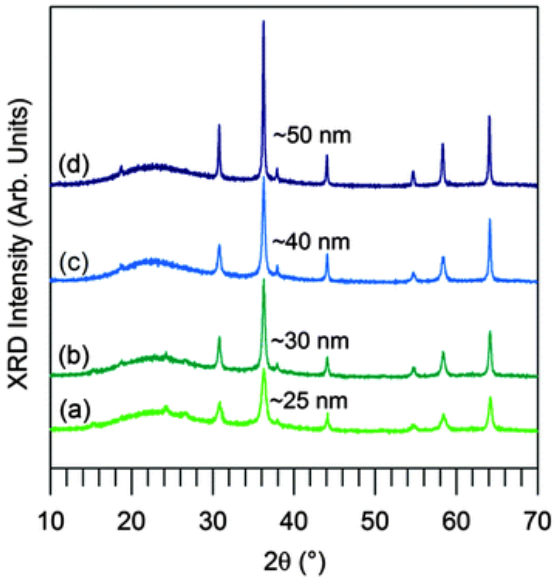

Fig. 8 XRD patterns of glass with molar composition, (a) $7.5Li_2O–2.5Na_2O–20Ga_2O_3–35GeO_2–35SiO_2$; (b) $7.5Li_2O–2.5Na_2O–20Ga_2O_3–35GeO_2–35SiO_2$ doped with 0.1NiO; (c) $10Li_2O–20Ga_2O_3–35GeO_2–35SiO_2$ doped with 0.1NiO; and (d) $7.5Li_2O–2.5Na_2O–20Ga_2O_3–35GeO_2–35SiO_2$ doped with 1NiO. The patterns are shifted for clarity. Samples were treated with the same heating rate as in DSC measurements from room temperature up to the temperatures indicated by open circles in the DSC curves in Fig. 1. The values indicated in the figure denote the size of $LiGa_5O_8$ NCs estimated from the XRD peak at about 64.2° by using the Scherrer's equation.

The registered endothermic peak extremum temperature T_{ep} shows a clear correlation with the NC size r as determined by the Scherrer analysis of the XRD patterns in Fig. 8. Interestingly, the analysis suggest a linear dependence of T_{ep} on $1/r$ (Fig. 9), reproduced by an equation of the form,

$$T_{ep} = T_{ep}^{bulk}\left(1-\frac{\varphi}{r}\right) \qquad (3)$$

where the intercept T^{bulk}_{ep} for $r \rightarrow \infty$ falls approximately in the same temperature range of the endothermic order–disorder transformation of bulk $LiGa_5O_8$. Such a dependence resembles the relationship describing the depression of melting temperature, with respect to bulk, observed in several nanosystems.[46–48] In that case, the constant φ is proportional to the difference $(\gamma_{sol} - \gamma_{liq})$ between surface energy in the solid and liquid phase.[47,49] Similarly to that situation, the difference $(\gamma_{ord} - \gamma_{dis})$ in surface energy between ordered and disordered $LiGa_5O_8$ polymorphs is expected to be positive – with a resulting lowering of T_{ep} at decreasing r – since a more ordered nanophase surface is likely associated with higher interface energy with the surrounding amorphous matrix.

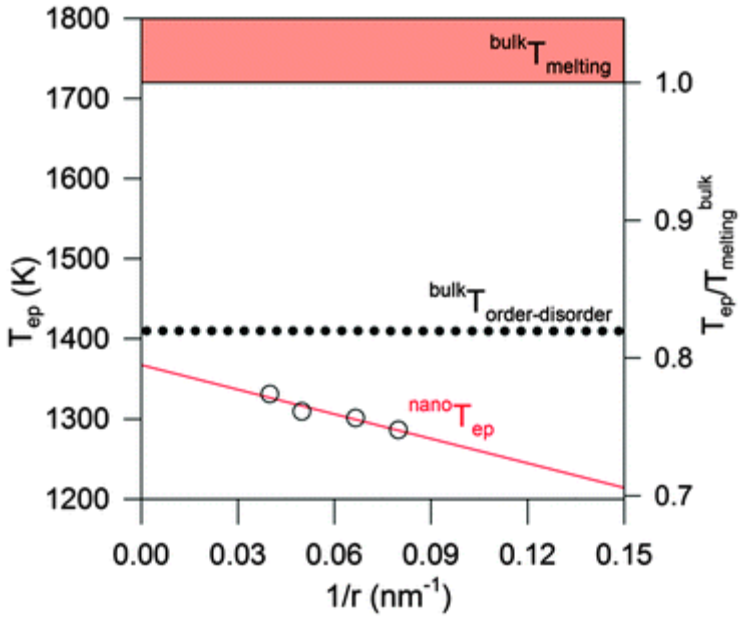

Fig. 9 NC size dependence of the endothermic peak extremum temperature T_{ep} in the set of nanocrystallized samples of Fig. 8. The full line is the linear fit of the data according to eqn (3). The melting temperature region (from literature) and reversible order–disorder transition temperature of bulk $LiGa_5O_8$ are also indicated.

Even though the data in Fig. 9 suggest a role of $LiGa_5O_8$ polymorphic transformation in determining the temperature of the endothermic peak, the polymorphic transformation cannot justify the full chain of events underlying the endothermic process. In fact, according to data in Fig. 4, the final product after the endothermic peak is not the high temperature $LiGa_5O_8$ polymorph but, rather, the formation of β-Ga_2O_3. Furthermore, the endothermic peak is not related to a reversible process.

Therefore, the full consideration of the available experimental results points to ascribe the endothermic process to the decomposition of $LiGa_5O_8$ NCs into β-Ga_2O_3, and Li_2O, promoted by the destabilization of NCs by $LiGa_5O_8$ polymorphic transformation at temperatures influenced by size effects and matrix interaction.

Photoluminescence of transformed nanocrystals

In Fig. 10 we present the results of photoluminescence measurements (using an excitation wavelength of 250 nm) on the nanostructured glass – compared with as-quenched glass – along the main steps of the nanophase thermal evolution. The spectral position and bandwidth are consistent with the luminescence observed in previous studies on pure Ga_2O_3 phases and Ga-oxide nanosystems, either pure or embedded in solid.[3,47,51] The broad and efficient luminescence excitation at wavelengths shorter than 280 nm is strictly related to the direct allowed optical gap of the material, and constitutes the most important optical feature for applications.[3] The mechanism of light emission is connected to the radiative recombination of donor and acceptor pairs consisting of an oxygen vacancy, acting as a donor, and a complex of oxygen and gallium vacancies behaving as acceptors.[3,47] Additional distinct spectral contributions in the green and UV regions are sometimes observed and can be respectively ascribed to electron–hole recombination between oxygen and gallium vacancies and to exciton-like decay mediated by sub-band gap levels.[51–54]

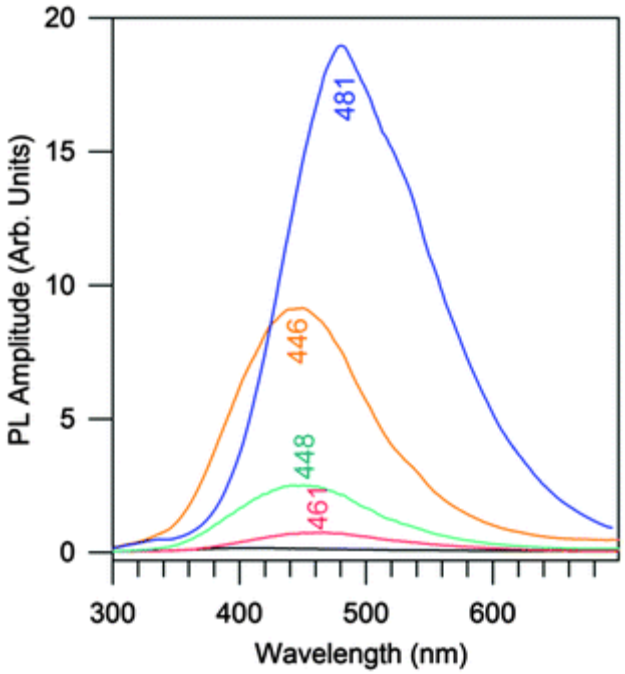

Fig. 10 Photoluminescence spectra of $7.5Li_2O–2.5Na_2O–20Ga_2O_3–35GeO_2–35SiO_2$ before (lower curve) and after heating for 15 min at 965 K (centred at 461 nm), 1 h at 990 K (centred at 448 nm), from 300 K to 1275 K at 10 K min^{-1} (centred at 446 nm), and for 1 h at 1285 K (centred at 481 nm). Spectra are collected under identical conditions, using an excitation wavelength of 250 nm, and signal intensity can be quantitatively compared within an uncertainty of 10%.

Looking at Fig. 10, we can notice two important features. First, we observe that the higher the treatment temperature, the higher is the luminescence intensity. Second, the spectral distribution of light emitted intensity shows a blue-shift at higher photon energy, except for the sample treated at the endothermic peak temperature (1285 K) where β-Ga_2O_3 is formed. In this sample the PL spectrum is red-shifted compared to the others. As regards the spectral shift, we have to remark that similar differences were observed among Ga-oxide phases, including alkali-containing compounds like $LiGa_5O_8$, but no definite explanation was ever proposed.[55,56]

Actually, attention should be paid in comparing our PL spectra with previously reported ones if collected in different excitation conditions, because the spectral shift can often occur as a result of excitation wavelength dependence. Nevertheless, within the set of spectra in Fig. 10 at fixed excitation at 250 nm, the observed shift provides a reliable evidence of changes occurring in the emitting nanophase. On the one hand, the phase transformation into β-Ga_2O_3 – whose crystal structure is largely different from the starting γ-Ga_2O_3 and $LiGa_5O_8$ spinel phases – may have a direct role in the change in spectral distribution because the structural environment of oxygen and gallium vacancies, responsible for light emission, is significantly modified. On the other hand, the spectral shifts accompanying heat treatments below the endothermic peak are instead more likely related to a different effect. On the basis of the studies already quoted on the origin of Ga-oxide light emissions,[3,50–54] the observed spectral changes are compatible with modified relative intensities of overlapping contributions from different light emitting sites, whose energy structure is probably quite independent of the small structural differences between γ-Ga_2O_3 and $LiGa_5O_8$ spinel phases. Such a modification is easily conceivable considering that the relative population of oxygen and gallium vacancies can significantly be modified during the thermal evolution of the system. The interaction with the surrounding matrix (with oxygen and lithium diffusion) and the NC coalescence (with change of surface-to-volume ratio) can indeed greatly modify the nanophase defectiveness. As a result, not only the spectral position of the PL band is affected by the treatment, but also the overall PL efficiency turns out to be influenced, even at a fixed amount of the separated phase. This is evident

from the two samples with the most intense spectra, in which the crystal fraction estimated from XRD patterns turns out to be equal to the nominal amount of Ga_2O_3 component in both cases, whereas the PL intensity differs by more than a factor of 2.

Conclusions

The thermal evolution of γ-Ga_2O_3 in the alkali–germanosilicate amorphous host shows the occurrence of transformation mechanisms, definitely distinct from those expected along the known evolution of the pure and freestanding phase, either in bulk or at the nanoscale, evidenced by an endothermic transformation previously uncharacterized. The results of DSC analysis, XRD and TEM characterizations provide clear-cut evidence of interactions with the surrounding matrix. After the exothermic process of γ-Ga_2O_3 nano-crystallization, the evolution of the nanophase is influenced, in a first step, by Li ion diffusion from the glass, which determines $LiGa_5O_8$ formation. In a second step, by increasing the temperature, size effects and the influence of the surrounding amorphous matrix on the interface energy induce an order-to-disorder $LiGa_5O_8$ change. The latter step, caused by a non negligible propensity of the high-temperature $LiGa_5O_8$ polymorph to dissociate, finally entails into an irreversible endothermic process with the formation of β-Ga_2O_3.

Photoluminescence measurements show modifications of spectral distribution and integrated intensity of the nanophase light emission, whose features are reflections of the overlapping contributions from donor–acceptor pair recombination and decay processes at defect sites.

Acknowledgements

This work has been supported by the Ministry of Education and Science of the Russian Federation under Grant No. 11.G34.31.0027 and by Grant MK-1398.2014.3, by Cariplo Foundation, Italy, under Project no. 2012-0920, and by ETH Zurich.

Notes and references

1. M. Wuttig and N. Yamada , *Nat. Mater.*, 2007, **6** , 824
2. L. Nagarajan , R. A. De Souza , D. Samuelis , I. Valov , A. Böger , J. Janek , K. D. Becker , P. C. Schmidt and M. Martin , *Nat. Mater.*, 2008, **7** , 391
3. V. N. Sigaev , N. V. Golubev , E. S. Ignat'eva , A. Paleari and R. Lorenzi , *Nanoscale*, 2014, **6** , 1763
4. V. N. Sigaev , N. V. Golubev , E. S. Ignat'eva , B. Champagnon , D. Vouagner , E. Nardou , R. Lorenzi and A. Paleari , *Nanoscale*, 2013, **5** , 299
5. S. V. Lotarev , A. S. Lipatiev , N. V. Golubev , E. S. Ignat'eva , G. E. Malashkevich , A. V. Mudryi , Yu. S. Priseko , R. Lorenzi , A. Paleari and V. N. Sigaev , *Opt. Lett.*, 2013, **38** , 492
6. J. Zhang , M. Gecevičius , M. Beresna and P. G. Kazansky , *Phys. Rev. Lett.*, 2014, **112** , 033901
7. A. Royon , K. Bourhis , M. Bellec , G. Papon , B. Bousquet , Y. Deshayes , T. Cardinal and L. Canioni , *Adv. Mater.*, 2010, **22** , 5282
8. S. S. Farvid and P. V. Radovanovic , *J. Am. Chem. Soc.*, 2012, **134** , 7015
9. L. N. Hutfluss and P. V. Radovanovic , *J. Am. Chem. Soc.*,
10. S. Huang , Z. Huang , W. Gao and P. Cao , *Inorg. Chem.*, 2013, **52** , 14188
11. H. Boucetta , R. Podor , L. Stievano , J. Ravaux , X. Carrier , S. Casale , S. Gossé , A. Monteiro and S. Schuller , *Inorg. Chem.*, 2012, **51** , 3478

12. N. Hu , H. Yu , M. Zhang , P. Zhang , Y. Wang and L. Zhao , *Phys. Chem. Chem. Phys.*, 2011, **13** , 1499
13. H. W. Choi , Y. H. Kim , Y. H. Rim and Y. S. Yang , *Phys. Chem. Chem. Phys.*, 2013, **15** , 9940
14. S. Brovelli , N. Chiodini , R. Lorenzi , A. Lauria , M. Romagnoli and A. Paleari , *Nat. Commun.*, 2012, **3** , 690
15. S. Zhou , C. Li , G. Yang , G. Bi , B. Xu , Z. Hong , K. Miura , K. Hirao and J. Qiu , *Adv. Funct. Mater.*, 2013, **23** , 5436
16. S. Zhou , N. Jiang , H. Dong , H. Zeng , J. Hao and J. Qiu , *Nanotechnology*, 2008, **19** , 015702
17. S. Zhou , N. Jiang , K. Miura , S. Tanabe , M. Shimizu , M. Sakakura , Y. Shimotsuma , M. Nishi , J. Qiu and K. Hirao , *J. Am. Chem. Soc.*, 2010, **132** , 17945
18. M. Zinkevich and F. Aldinger , *J. Am. Ceram. Soc.*, 2004, **87** , 683
19. H. Y. Playford , A. C. Hannon , E. R. Barney and R. I. Walton , *Chem. – Eur. J.*, 2013, **19** , 2803
20. M. R. Delgado and C. O. Areán , *Z. Anorg. Allg. Chem.*, 2005, **631** , 2115
21. J. P. Remeika and M. Marezio , *Appl. Phys. Lett.*, 1966, **8** , 87
22. C. O. Areán , A. L. Bella , M. P. Mentruit , M. R. Delgado and G. T. Palomino , *Microporous Mesoporous Mater.*, 2000, **40** , 35
23. L. Li , W. Wie and M. Behrens , *Solid State Sci.*, 2012, **14** , 971
24. H. Y. Playford , A. C. Hannon , M. G. Tucker , D. M. Dawson , S. E. Ashbrook , R. J. Kastiban , J. Sloan and R. I. Walton , *J. Phys. Chem. C*, 2014, **118** , 16188
25. N. Pinna , G. Garnweitner , M. Antonietti and M. Niederberger , *J. Am. Chem. Soc.*, 2005, **127** , 5608
26. T. Wang , S. S. Farvid , M. Abulikemu and P. V. Radovanovic , *J. Am. Chem. Soc.*, 2010, **132** , 9250
27. M. Zinkevich , F. M. Morales , H. Nitsche , M. Ahrens , M. Rühle and F. Aldinger , *Z. Metallkd.*, 2004, **95** , 756
28. R. Roy , V. G. Hill and E. F. Osborn , *J. Am. Chem. Soc.*, 1952, **74** , 719
29. S. Zhou , H. Dong , G. Feng , B. Wu , H. Zeng and J. Qiu , *Opt. Express*, 2007, **15** , 5477
30. S. Zhou , G. Feng , B. Wu , N. Jiang , S. Xu and J. Qiu , *J. Phys. Chem. C*, 2007, **111** , 7335
31. B. Wu , S. Zhou , J. Ren , D. Chen , X. Jiang , C. Zhu and J. Qiu , *Appl. Phys. B: Lasers Opt.*, 2007, **87** , 697
32. S. Xu , D. Deng , R. Bao , H. Ju , S. Zhao , H. Wang and B. Wang , *J. Opt. Soc. Am. B*, 2008, **25** , 1548
33. V. N. Sigaev , N. V. Golubev , E. S. Ignat'eva , V. I. Savinkov , M. Campione , R. Lorenzi , F. Meinardi and A. Paleari , *Nanotechnology*, 2012, **23** , 015708
34. S. Chenu , E. Véron , C. Genevois , G. Matzen , T. Cardinal , A. Etienne , D. Massiot and M. Allix , *Adv. Opt. Mater.*, 2014, **2** , 364
35. T. Suzuki , G. S. Murugan and Y. Ohishi , *Appl. Phys. Lett.*, 2005, **86** , 131903
36. T. Suzuki , Y. Arai and Y. Ohishi , *J. Non-Cryst. Solids*, 2007, **353** , 36
37. S. Zhou , N. Jiang , B. Wu , J. Hao and J. Qiu , *Adv. Funct. Mater.*, 2009, **19** , 2081
38. J. Åhman , G. Svensson and J. Albertsson , *Acta Chem. Scand.*, 1996, **50** , 391
39. R. Lorenzi , A. Paleari , N. V. Golubev , E. S. Ignat'eva , V. N. Sigaev , M. Niederberger and A. Lauria , *J. Mater. Chem. C*, 2015, **3** , 41
40. R. K. Datta *J. Am. Ceram. Soc.*, 1971, **54** , 262
41. N. Reeves , D. Pasero and A. R. West , *J. Solid State Chem.*, 2007, **180** , 1894
42. A. Khawam and D. F. Flanagan , *J. Phys. Chem. B*, 2006, **110** , 17315
43. C. W. W. Hoffman and J. J. Brown , *J. Inorg. Nucl. Chem.*, 1968, **30** , 63
44. M. L. Meylman *Opt. Mater.*, 2006, **28** , 221
45. G. K. Abdullaev , P. F. Rzazade and K. S. Mamedov , *Zh. Neorg. Khim.*, 1984, **29** , 2387

46. V. I. Levitas and K. Samani , *Nat. Commun.*, 2011, **2** , 284
47. Q. Jiang and C. C. Yang , *Curr. Nanosci.*, 2008, **4** , 179
48. T. P. Martin , U. Näher , H. Schaber and U. Zimmermann , *J. Chem. Phys.*, 1994, **100** , 2322
49. P. R. Couchman and W. A. Jesser , *Nature*, 1977, **269** , 481
50. L. Binet and D. Gourier , *J. Phys. Chem. Solids*, 1998, **59** , 1241
51. M. Hegde , T. Wang , Z. L. Miskovic and P. V. Radovanovic , *Appl. Phys. Lett.*, 2012, **100** , 141903
52. J. Díaz , I. López , E. Nogales , B. Méndez and J. Piqueras , *J. Nanopart. Res.*, 2011, **13** , 1833
53. K. Shimamura , E. G. Víllora , T. Ujiie and K. Aoki , *Appl. Phys. Lett.*, 2008, **92** , 201914
54. Z. Liu , X. Jing and L. Wang , *J. Electrochem. Soc.*, 2007, **154** , H440
55. Y. Hou , L. Wu , X. Wang , Z. Ding , Z. Li and X. Fu , *J. Catal.*, 2007, **250** , 12
56. G. Blasse and A. Bril , *Mater. Res. Bull.*, 1970, **5** , 231